Volume 5
Number 2
21 January 2024
Pages 381–832

Materials Advances

rsc.li/materials-advances

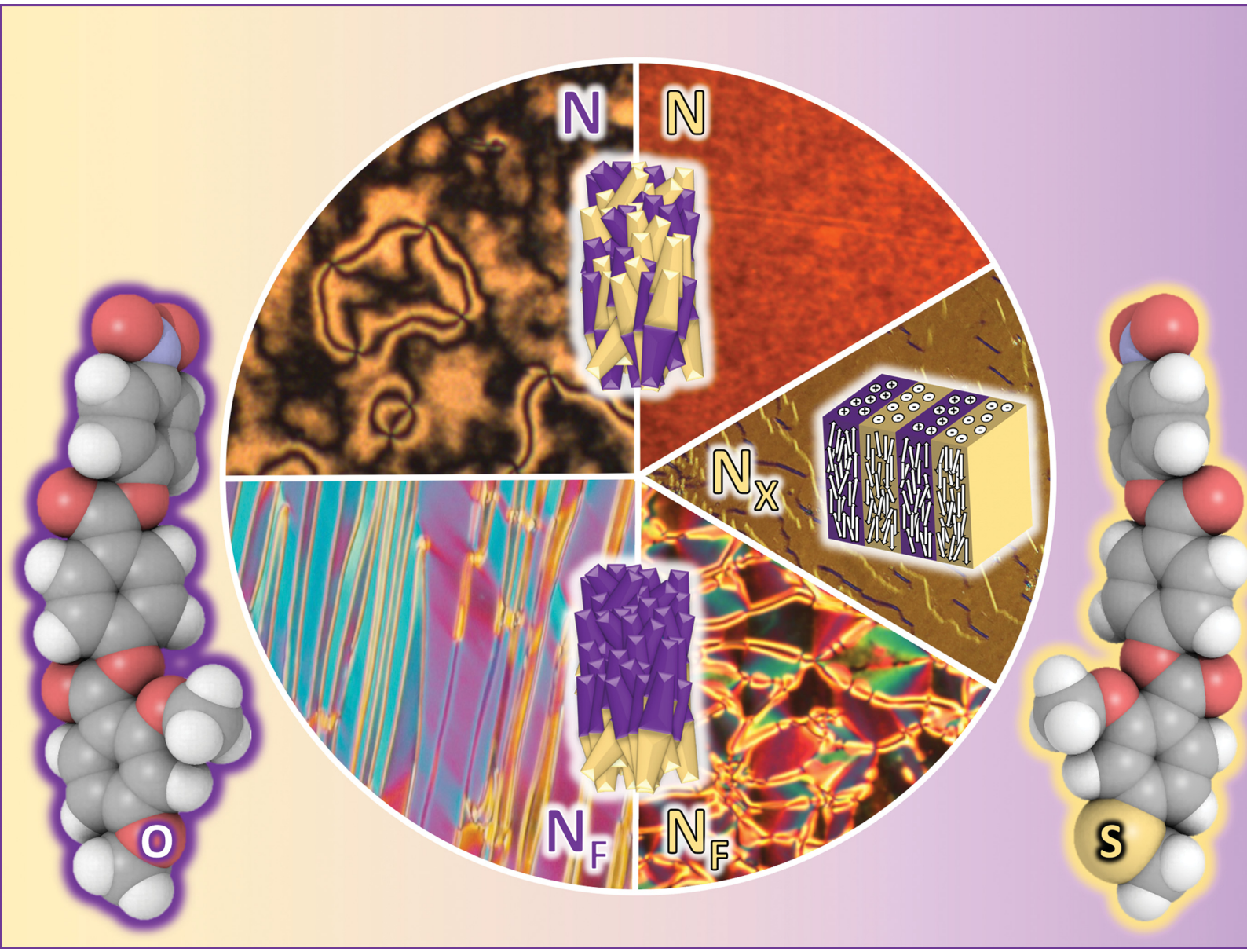

ISSN 2633-5409

ROYAL SOCIETY OF CHEMISTRY

PAPER
Ewan Cruickshank *et al.*
Ferroelectric nematogens containing a methylthio group

Materials Advances

ROYAL SOCIETY OF CHEMISTRY

PAPER

View Article Online
View Journal | View Issue

Cite this: *Mater. Adv.*, 2024, 5, 525

Ferroelectric nematogens containing a methylthio group†

Gytis Stepanafas, [a] Ewan Cruickshank, ‡*[a] Stevie Brown, [a] Magdalena M. Majewska, [b] Damian Pociecha, [b] Ewa Gorecka, [b] John M.D. Storey [a] and Corrie T. Imrie [a]

The synthesis and characterisation of eight nematogens containing a terminal methylthio group is reported. The compounds are based on RM734 and differ in the number and position of fluorine substituents, and in the position of the lateral methoxy substituent. Seven of these compounds exhibit a monotropic ferroelectric nematic phase, N_F, including examples of N_F-isotropic phase transitions. Two of the compounds show the anti-ferroelectric N_X phase. Their transitional behaviour is discussed in terms of molecular shape and changes in electronic properties. Their phase behaviour is similar to that of the corresponding compounds containing a terminal methoxy group, but the methoxy terminated materials consistently show the higher transition temperatures. This is accounted for by the larger reduction in molecular shape anisotropy associated with the methylthio group, and the associated change in the electronic properties. The N_X phase seen for the methylthio substituted compounds are thought to reflect the suppression of the N_F phase by the methylthio group rather than any specific stabilising effect. Specific interactions between methylthio groups thought to stabilise nematic behaviour do not appear to stabilise the N_F phase.

Received 21st July 2023,
Accepted 14th October 2023

DOI: 10.1039/d3ma00446e

rsc.li/materials-advances

Introduction

The ferroelectric nematic phase, N_F, was experimentally discovered in 2017,[1–3] and is now the hottest topic in liquid crystal research. In the conventional nematic phase, N, the rod-like molecules are more or less aligned along a common direction, the director, whereas their centres of mass are distributed randomly. The director is described by a unit vector, $\boldsymbol{n}$, which possesses inversion symmetry such that $\boldsymbol{n} = -\boldsymbol{n}$, and the phase is apolar, Fig. 1. In the N_F phase, the director no longer possesses inversion symmetry *i.e.* $\boldsymbol{n} \neq -\boldsymbol{n}$, and the phase is polar, Fig. 1.[4] This phase has generated very significant excitement not only given the fundamental importance of a fluid ferroelectric phase, but also because it has huge application potential in a range of electrooptic technologies. A small number of materials exhibit a further liquid crystal phase referred to as the N_X or SmZ_A phase.[2,5–8] The N_X phase is thought to consist of regions of polar nematic phase arranged in a regular antiferroelectric structure.[5,7,9]

To date there have been around 150 molecules reported to show the N_F phase and bar a handful of exemptions such as polymers,[10,11] these materials may be described as conventional low molar mass mesogens.[3,6,8,12–25] The empirical structure–property relationships describing the links between the formation of the N_F phase and molecular structure have yet to be established let alone understood. The archetypal ferroelectric nematic compounds RM734[3] and DIO[2] have large longitudinal dipole moments and possess lateral bulk in the form of either a methoxy group or fluorine substituents. It has been

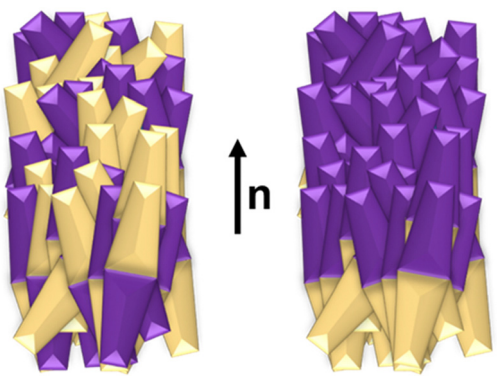

Fig. 1 Schematic representations of the conventional nematic, N, phase (left) and ferroelectric nematic, N_F, phase (right).

[a] Department of Chemistry, University of Aberdeen, Old Aberdeen, AB24 3UE, UK. E-mail: ewan.cruickshank2@abdn.ac.uk
[b] Faculty of Chemistry, University of Warsaw, ul. Zwirki i Wigury 101, 02-089, Warsaw, Poland

† Electronic supplementary information (ESI) available. See DOI: https://doi.org/10.1039/d3ma00446e

‡ Present Address: School of Pharmacy and Life Sciences, Robert Gordon University, Aberdeen, AB10 7GJ, U.K.

suggested that these structural factors are prerequisites for the observation of the N_F phase. Indeed, this view is supported by computer simulations of tapered Gay–Berne particles possessing longitudinal dipole moments that revealed N_F behaviour.[26] Exceptions have been reported to these generalisations (see, for example, ref. 18,24,27), and in order to design new ferroelectric nematogens having tailored properties in a rational manner we must first explore and understand the relationships between structure and properties for the N_F phase.

Sulfur has been used extensively in the design of liquid crystals including, for example, in terminal alkylthio chains,[28–34] alkylthio spacers,[35–40] thiophene moieties,[41–44] thiocyanate terminal groups,[45,46] and thioester linking groups.[47,48] One driving force for this research is the enhanced values of optical birefringence exhibited by compounds that contain sulfur.[45,49–52] Highly birefringent nematogens have considerable application potential not only in liquid crystal display technologies, but also have an important role to play in emerging technologies such as liquid crystal lenses[53,54] and as holographic materials.[55] Surprisingly, sulfur has very largely been overlooked in the design of ferroelectric nematogens, and to address this surprising omission, here we report the synthesis and characterisation of eight new compounds, **S1–8**, designed to exhibit the N_F phase and that contain a methylthio substituent, Table 1. These are based on the archetypal ferroelectric nematogen RM734.[3] The properties of these compounds are compared with those of the corresponding materials in which the methylthio group has been replaced by a methoxy unit, **O1–8**, Table 1. We note that **O1** is RM734. Critically, this is the first time that specifically the effect of replacing the terminal methoxy group with a terminal methylthio group on the formation of the N_F phase has been studied, while also sequentially changing the degree of fluorination incorporated into the molecular backbone.

Experimental

Synthesis

The synthetic route used to prepare **S1–8** is shown in Scheme 1 and for **O5** and **O6** in Scheme 2. A detailed description of the preparation of these compounds, including the structural characterisation data for all intermediates and final products, is provided in the Supplementary Information.

Optical studies

Phase characterisation was performed by polarised light microscopy, using an Olympus BH2 polarising light microscope equipped with a Linkam TMS 92 hot stage. Slides treated for planar alignment were purchased from INSTEC or AWAT with a thickness between 2.9–3.5 μm or 1.8 μm, respectively and both sets of cells were ITO conducting.

Differential scanning calorimetry

The phase behaviour of the materials was studied by differential scanning calorimetry performed using a Mettler Toledo DSC1 or DSC3 differential scanning calorimeter equipped with TSO 801RO sample robots and calibrated using indium and zinc standards. Heating and cooling rates were 10 K min^{-1}, with a 3 min isotherm between either heating or cooling, and all samples were measured under a nitrogen atmosphere. Transition temperatures and associated enthalpy changes were extracted from the heating traces unless otherwise noted. For each sample, two aliquots were measured, and the data listed are the average of the two sets of data.

Molecular modelling

The geometric parameters of the reported compounds were obtained using quantum mechanical DFT calculations with Gaussian09 software.[56] Optimisation of the methylthio-containing structures (**S1–8**) was carried out at the B3LYP/6-311G(d,p) level of theory. Comparison of the results of optimisation of the corresponding ether-linked (**O1–8**) materials at the B3LYP/6-311G(d,p) and the 6-31G(d) levels showed no discernible difference in the geometries found, and so their optimisation was carried out at the B3LYP/6-31G(d) level. Visualisations of the electronic surfaces were generated from the optimised geometries using the GaussView 5 software, and visualisations of the space-filling models were produced post-optimisation using the QuteMol package.[57]

Birefringence measurements

Birefringence was measured with a setup based on a photoelastic modulator (PEM-90, Hinds) working at a modulation frequency f = 50 kHz; as a light source, a halogen lamp (Hamamatsu LC8) was used equipped with narrow bandpass filters (633 nm and 690 nm). The signal from a photodiode (FLC Electronics PIN-20) was deconvoluted with a lock-in amplifier (EG&G 7265) into 1f and 2f components to yield a retardation induced by the sample. Knowing the sample thickness, the retardation was recalculated into optical birefringence. Samples were prepared in 4.9-micron-thick cells with planar anchoring. The alignment quality was checked prior to measurement by inspection under the polarised light optical microscope.

Spontaneous electric polarization measurements

Values of the spontaneous electric polarization were obtained from the current peaks recorded during Ps switching upon applying a triangular-wave voltage at a frequency of 2 Hz. The 9.7 μm-thick cells with ITO electrodes and no polymer aligning layers were used and the switching current was determined by recording the voltage drop at the resistivity of 50 kΩ in serial connection with the sample. The current peak was integrated over time to calculate the surface electric charge and evaluate the polarization value.

Dielectric spectroscopy

The complex dielectric permittivity, ε^*, was studied using a Solatron 1260 impedance analyser. Measurements were conducted in the 1 Hz–1 MHz frequency (f) range, with the probe voltage of 20 mV, and it was checked by optical observations that such a voltage is below the Fredericks transition threshold. The material was placed in 9.7 μm-thick glass cells with ITO electrodes and no polymer aligning layers. Lack of a surfactant

Table 1 Molecular structures of the S*n* and O*n* compounds

Name	Structure	Name	Structure
S1	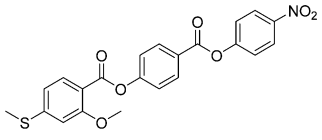	**O1**	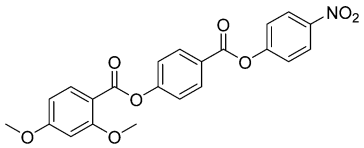
S2	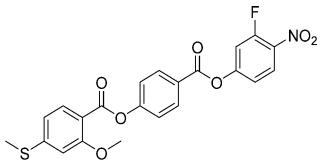	**O2**	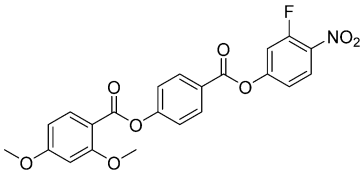
S3	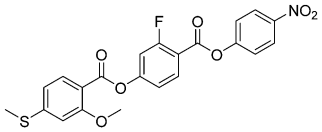	**O3**	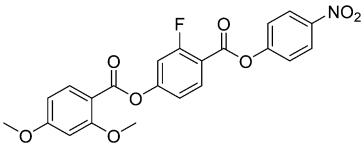
S4	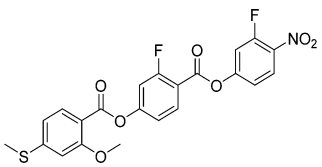	**O4**	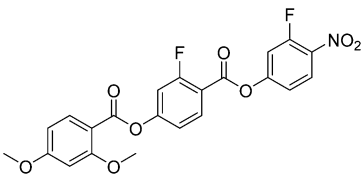
S5	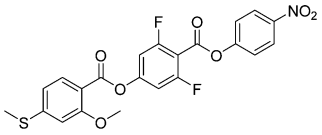	**O5**	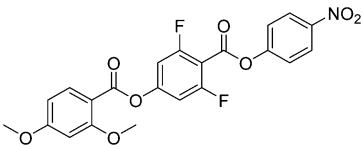
S6	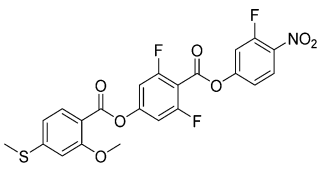	**O6**	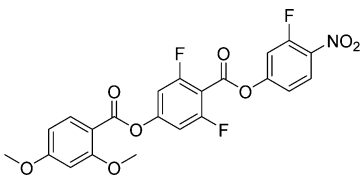
S7	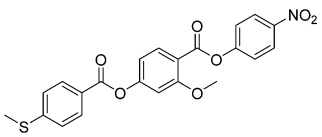	**O7**	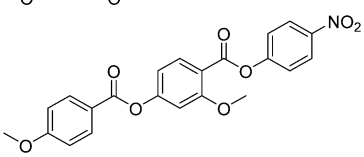
S8	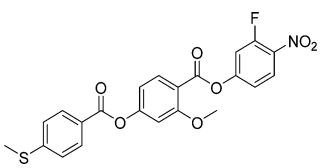	**O8**	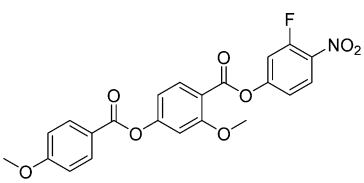

layer resulted in the random configuration of the director in the LC phases; microscopic observations of optical textures suggested a dominant planar orientation without preferable direction of the long molecular axis. The relaxation frequency, f_r, and dielectric strength of the mode, $\Delta\varepsilon$, were evaluated by fitting the complex dielectric permittivity to the Cole–Cole formula:

$$\varepsilon - \varepsilon_\infty = \sum \frac{\Delta\varepsilon}{\left(1 + \frac{if}{f_r}\right)^{1-\alpha}} + i\left(\frac{\delta}{2\pi\varepsilon_0 f}\right),$$

where ε_∞ is the high frequency dielectric constant, α is the distribution parameter of the mode and δ is the low frequency conductivity, respectively.

X-ray diffraction

The X-ray diffraction (XRD) measurements were performed with a Bruker D8 GADDS system (CuKα line, Goebel mirror, point beam collimator, Vantec2000 area detector). The temperature of the sample was controlled with precision of $\pm$0.1 K. Samples were prepared as droplets on a heated surface.

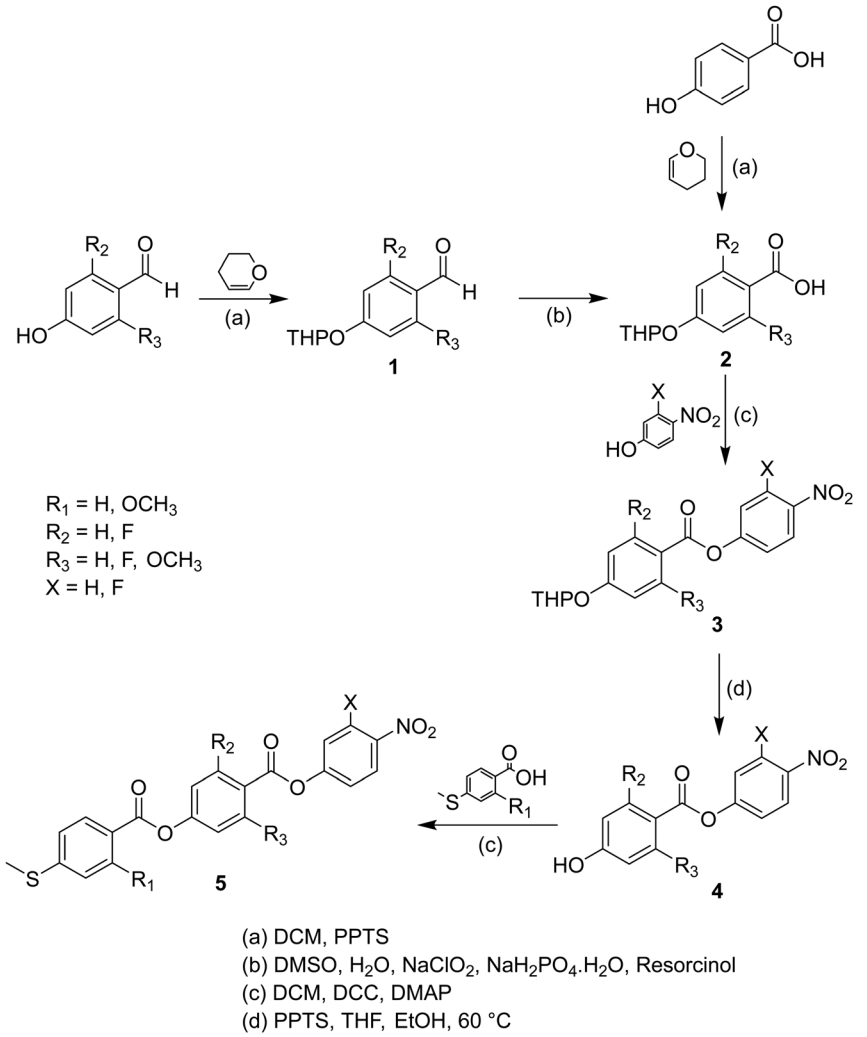

Scheme 1 Synthetic route used to obtain the S*n* compounds.

Results and discussion

The transitional properties of the methylthio-containing S*n* materials are listed in Table 2. The conventional nematic phase, N, was assigned based on the observation of a characteristic uniform texture in a cell treated for planar alignment, Fig. 2(a), or on the observation of a characteristic schlieren texture containing two- and four-brush point defects when the sample was sandwiched between two untreated glass slides, Fig. 3(a). These textures flashed when subjected to mechanical stress. For **S1** and **S7** on cooling the uniform texture of the nematic phase, a chevron pattern was observed at the transition to the N_X phase, Fig. 2(b). In XRD studies (these will be discussed in more detail later) the N_X phase shows only short-range correlations of the molecular positions which are characteristic for nematic phases and hence why the phase is named as such. However, in previous diffraction experiments performed at synchrotron facilities very weak Bragg-type diffraction signals were detected in the N_X phase,[9] revealing a kind of long-range periodicity. This periodicity was attributed to existence of regular domains with antiparallel orientation of the polarization, and so this phase is referred to by other groups as the antiferroelectric SmZ_A phase.[5–7] Cooling **S1** from the N_X phase saw a series of twisted states emerge a few degrees below the transition to the N_F phase, Fig. 2(c)–(e), and we have previously reported observing these textures for the N_F phase.[8] There was also a clear change in birefringence which is also considered characteristic of the N_F phase. In **S4** and **S6**, the N_F phase formed directly from the isotropic phase. In thicker cells treated for planar alignment, spherical droplets developed at the N_F-I transition and coalesced to form banded textures which are also characteristic of the N_F phase, Fig. 3(b) and (c).[10,13,18,20,25] This banded texture is observed due to the domains which form within the cell separated by distinct domain boundaries. These domains show regions in which the director has different orientations and so the polarisation direction is similarly changed. The banding within the domains is due to areas of lower and higher birefringence, with the domains themselves thought to form due to director splay deformations which are necessary to connect opposite polarisation vectors on the lower and upper

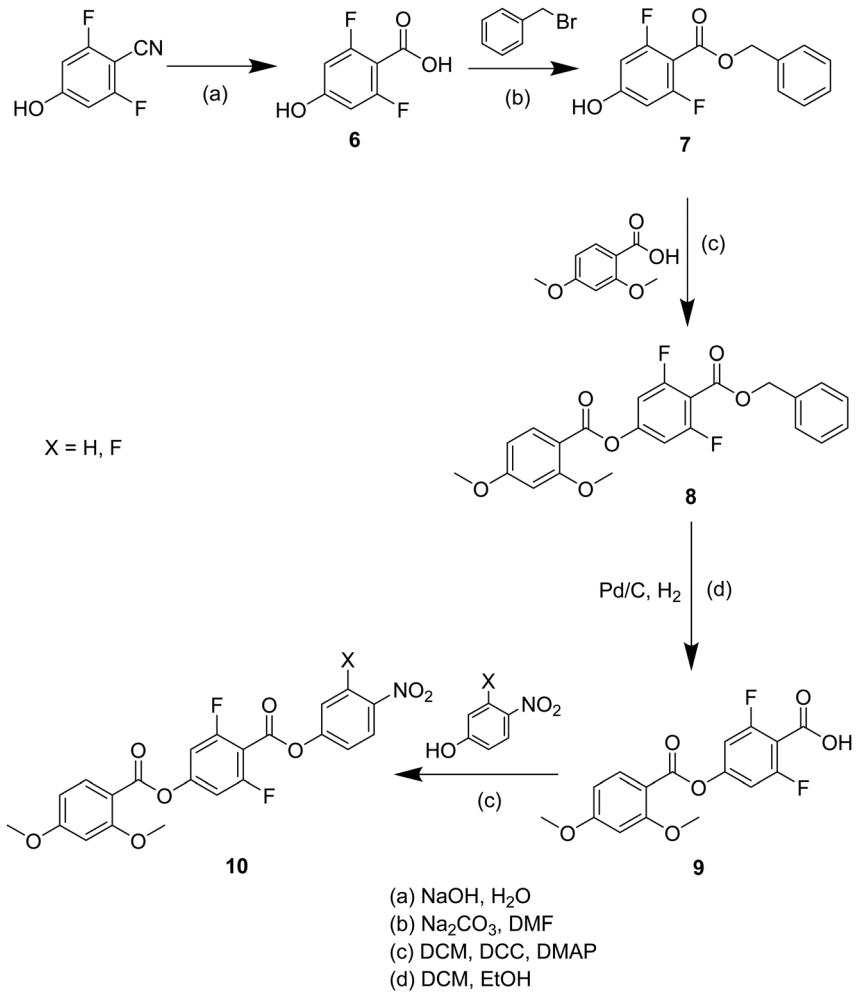

Scheme 2 Synthetic route used to obtain compounds **O5** and **O6**.

Table 2 Transition temperatures for the S*n* and O*n* series (in °C) with their associated enthalpy changes (in parentheses, kJ mol^{-1})

Compound	M.P.	Phase sequence
S1	147 (38.6)	I-169 (0.54)-N-[a]111 ([c]0.43)-N_X-[a]106 ([c]0.43)-N_F
S2	147 (43.9)	I-[a]135 (0.54)-N-[a]122 (1.29)-N_F
S3	162 (40.3)	I-[a]152 (0.41)-N-[a]126 (0.57)-N_F
S4	150 (36.0)	I-[a]129 (3.09)-N_F
S5	174 (47.8)	I-[a]127 (0.40)-N-[a]121 (0.80)-N_F
S6	171 (52.9)	I-[a]122 (3.56)-N_F
S7	164 (47.9)	I-172 (1.22)-N-[b]97-N_X
S8	164 (40.3)	I-[a]143 (0.74)-N-[a]124 (0.28)-N_F
[d]**O1**	139 (34.3)	I-188 (0.61)-N-131 (0.60)-N_F
[e]**O2**	166 (50.4)	I-155 (0.50)-N-140 (1.61)-N_F
[f]**O3**	161 (54.1)	I-165 (0.69)-N-143 (1.38)-N_F
[f]**O4**	151 (53.2)	I-139 (4.38)-N_F
O5	192 (50.6)	I-[a]139 (0.34)-N-[a]132 (1.62)-N_F
O6	160 (45.4)	I-[a]131 (4.33)-N_F
[g]**O7**	192 (48.3)	I-189 (0.81)-N-126 (0.11)-N_F
[g]**O8**	180 (51.6)	I-157 (10.4)-N-142 (1.17)-N_F

[a] Values extracted from DSC cooling traces. [b] Measured using the polarised light microscope. [c] Combined ΔH value associated with both phase transitions due to peak overlap in the DSC trace. [d] Data extracted from Cruickshank *et al.*[20] [e] Data extracted from Mandle *et al.*[3] [f] Data extracted from Brown *et al.*[8] [g] Data extracted from Tufaha *et al.*[18]

cell surfaces.[8] The scaled entropy changes, calculated using the enthalpy changes listed in Table 2, associated with the N_F–I transitions of **S4** and **S6** are several times larger than those associated with the N–I transitions, Table 2. This presumably reflects the additional entropic contribution associated with the ordering of the dipoles in the N_F phase compared to the conventional N phase. The values of the enthalpy changes listed in Table 2 are similar to those reported for other ferroelectric nematogens.[8,12,18,20]

In order to confirm the phase assignments, dielectric measurements were undertaken using **S1**. In the N phase, a clear dielectric mode was found for which the relaxation frequency decreased and the strength increased on cooling, as the correlation length of polar order also increased. There was a clear increase in the value of ε upon entry to the N_F phase, Fig. 4. The low frequency dielectric strength was over 10 000 and this is in agreement with values reported for other ferroelectric nematogens.[2,8,10,12,14–16,18,58–60] However, it has been recently reported that there may be a relationship between these values and the cell thickness.[61] The polar character of the N_F phase was further confirmed by the polarisation switching behaviour. When an AC voltage was applied a

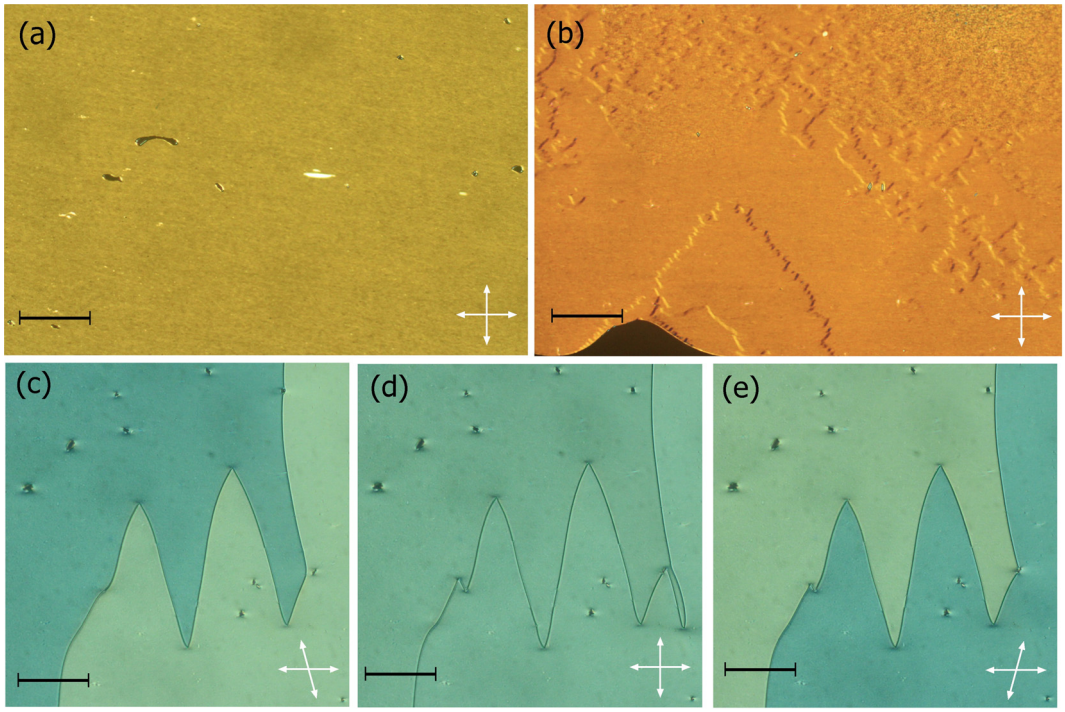

Fig. 2 Polarised optical microscope textures observed for the compound, **S1**: (a) uniform texture of the N phase at 130 °C; (b) chevron texture of the N_X phase at 110 °C; (c)–(e) twisted states of the N_F phase at 100 °C, with (d) showing the texture when the polarisers are fully crossed. All textures were obtained in cells treated for planar alignment with the scale bars each representing 200 μm.

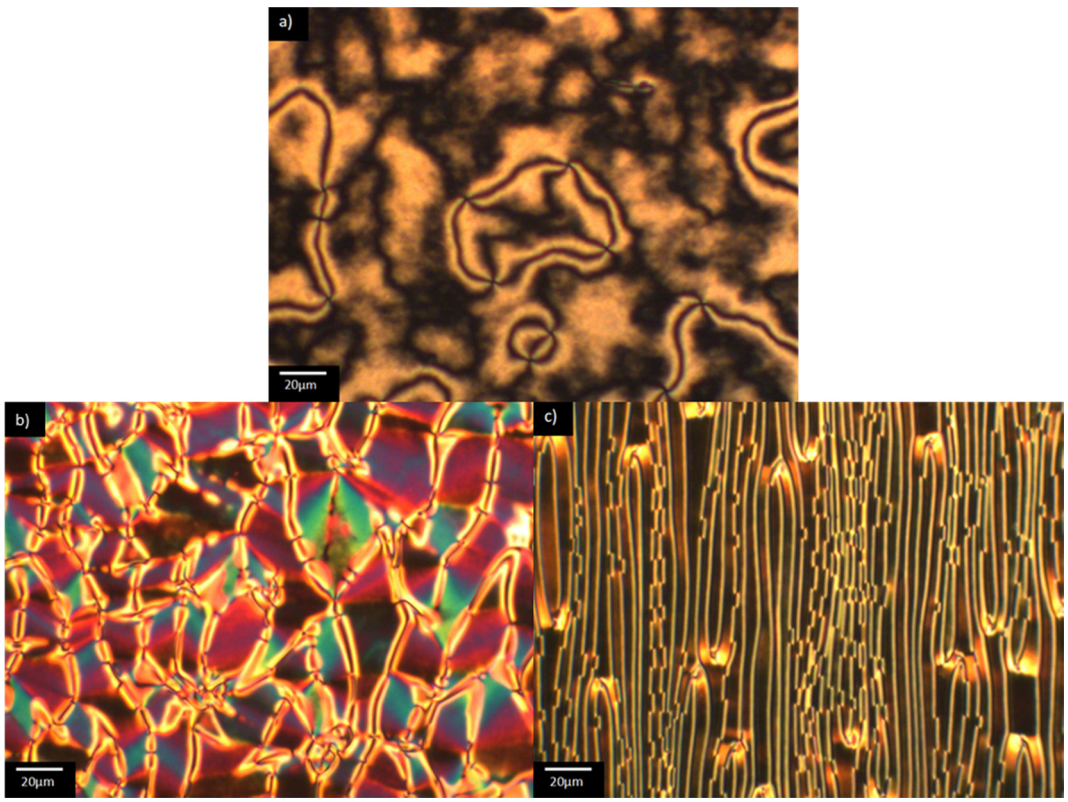

Fig. 3 Polarised optical microscope textures observed for the S*n* series: (a) schlieren texture of the N phase viewed between untreated glass slides for **S2** at 130 °C; (b) banded texture of the N_F phase viewed in a cell treated for planar alignment for **S2** at 122 °C; and (c) banded texture of the N_F phase viewed in a cell treated for planar alignment for **S6** at 110 °C.

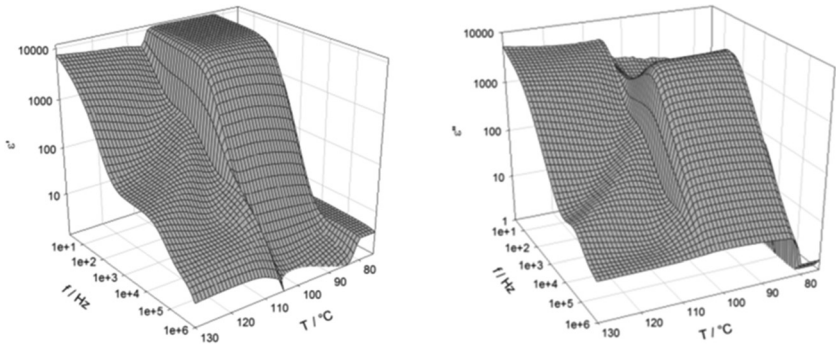

Fig. 4 Real (left) and imaginary (right) parts of the complex dielectric permittivity measured as a function of temperature and frequency for **S1**, in a 9.7 μm-thick cell with ITO electrodes and no alignment layer.

single current peak per half cycle was registered and this corresponded to a large spontaneous polarisation of 3.1 μC cm^{-2}, Fig. 5, but only around half the value reported for RM734.[4] Although these measurements gave a clear indication of **S1** exhibiting the ferroelectric nematic phase, they do not clearly reveal the N_X phase between the N and N_F phases that was seen using polarised light optical microscopy. The temperature dependence of the optical birefringence for **S1** is shown in Fig. 6. The optical studies showed that when the sample is cooled from the isotropic to the nematic phase, there is a sharp increase in the birefringence at the transition that then follows a critical power-law dependence. At the transition to the N_X phase there is a small change in the temperature dependence of birefringence showing that the phase is orientationally similar to the conventional nematic phase. This is followed by a small step-like increase at the transition to the N_F phase, indicative of an increase of the order parameter, *S*. This observation is in agreement with the birefringence measurements that we have reported previously for the N_X phase,[8,9] also referred to as the smectic Z_A phase.[5,62] Based on both the textural observations and this change in birefringence, the N_X phase in **S1** may be assigned as being the same phase shown by DIO and some related

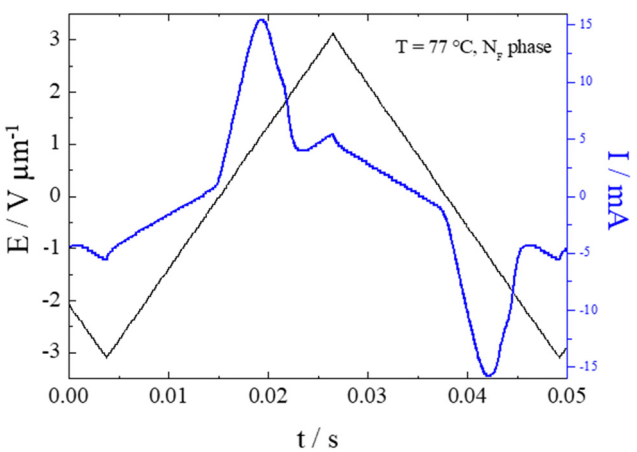

Fig. 5 The switching current (blue line) associated with polarization reversal under applied triangular wave voltage (black line) for **S1** at 77 °C. Measurements were performed in a 9.7 μm-thick cell with ITO electrodes and no alignment layer.

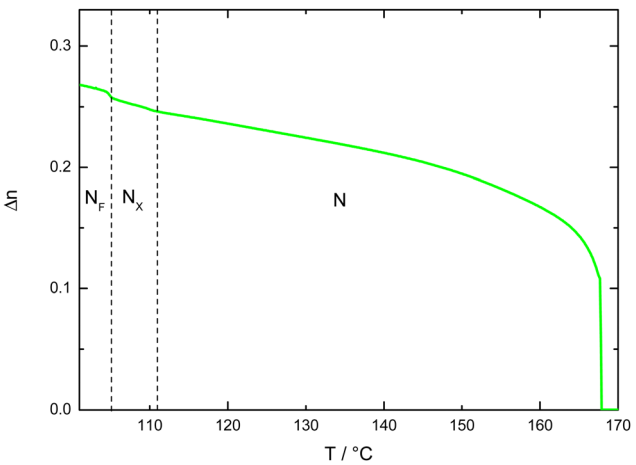

Fig. 6 Optical birefringence of **S1** measured with green light (λ = 532 nm) across the phase transitions with the light green line showing the birefringence measured on cooling.

compounds.[2,6,21] X-ray diffraction was also used to confirm the assignment of the phases in compound **S1** as nematics, Fig. 7. The X-ray diffraction patterns obtained for both the N and N_X phases are essentially identical consisting of broad signals indicative of there being only short-range correlations of the molecular positions. Prior to the observation of the N_F phase, however, the sample crystalised as shown by the observed diffraction pattern, Fig. 7 (c). The pattern seen for the N_X phase, although not showing the long-range periodicity we have reported previously,[9] does support its assignment as a nematic phase.

We now turn our attention to the dependence of the transition temperatures on molecular structure for the methylthio-substituted compounds listed in Table 2. **S1**, the methylthio-substituted analogue of the extensively studied RM734, shows the phase sequence N_F-N_X-N-I, and forms the basis of comparison for compounds **S2–6** in which one, two or three fluorine substituents are added to the structure. In **S2** a fluorine substituent has been added *ortho* to the nitro group and this has reduced the nematic–isotropic transition temperature, T_{NI}, by 34 K. This decrease is presumably associated with the reduction in shape anisotropy. Conversely, the ferroelectric nematic-nematic transition temperature, T_{NFN}, of **S2** is 16 K higher than that of the N_F–N_X

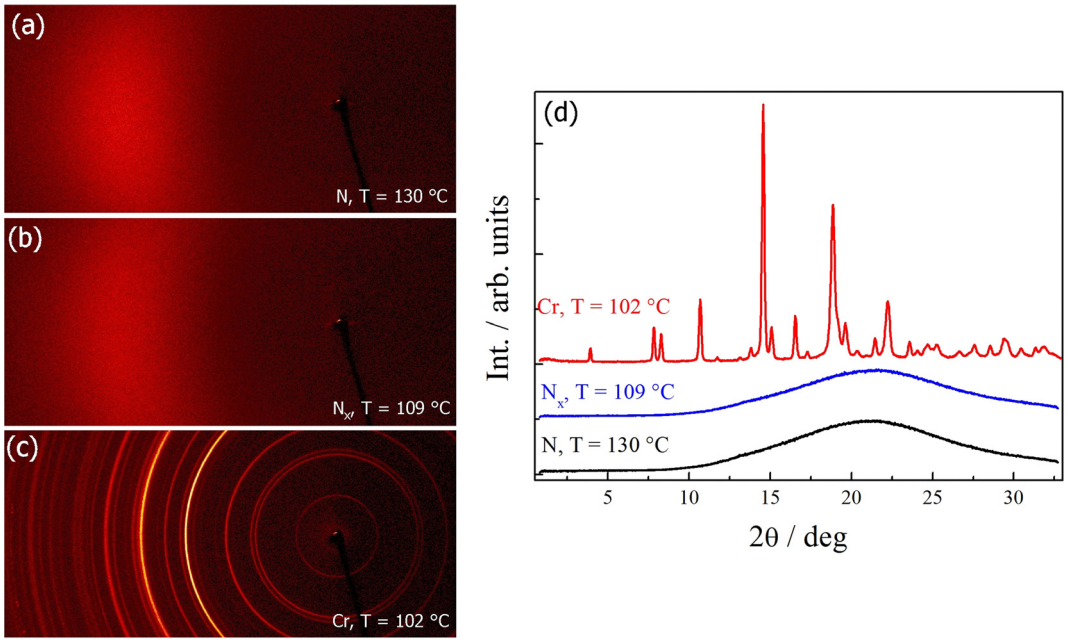

Fig. 7 X-ray diffraction patterns of compound **S1** in the (a) N phase; (b) N_X phase and (c) crystalline solid phase. (d) Intensity profiles of the X-ray patterns of the N phase (black line), N_X phase (blue line) and crystalline solid phase (red line).

transition temperature, T_{NFNX} observed for **S1**. This increase in the stability of the N_F phase may be attributed, in part, to an increase in the molecular dipole moment from 10.5 D for **S1** to 11.6 D for **S2**. It has also been suggested,[18] however, that this observation is consistent with the predictions of a molecular model developed by Madhusudana to describe the N_F phase in which the molecules are described by a longitudinal surface charge density wave.[63] Specifically, the model suggests that the parallel alignment of the molecules is enhanced by minimising the amplitude of the charge density wave at either end of the molecule. The addition of the fluorine atom *ortho* to the nitro group spreads the electron charge distribution reducing the amplitude of the charge density wave, and so predicted to increase the stability of the N_F phase as observed.

In **S3** a fluorine atom has been added to the central phenyl ring in **S1** and this reduces T_{NI} by 17 K. This is a much smaller reduction in T_{NI} than seen between **S1** and **S2** of 34 K and reflects the different contributions to the molecular shape arising from substitutions in differing positions, Fig. 8. Again, the addition of a fluorine atom sees an increase in the stability of the N_F phase and T_{NFN} for **S3** is some 20 K higher than T_{NFNX} observed for **S1**. This is a larger difference than seen between the corresponding values of **S2** and **S1** although the dipole moment of **S3** is 11.2 D and lies between those of **S1** and **S2**. Indeed, T_{NFN} for **S3** is higher than that of **S2** although we note that this is a small difference, just 4 K. This supports the view that the stability of the N_F phase cannot be simply associated with the magnitude of the molecular dipole moment. Within Madhusudana's model, the addition of the fluorine atom increases the amplitude of the charge density on the central ring and in relative terms decreases that associated with the terminal rings. Such a change is predicted to increase the stability of the N_F phase.

S4 contains two fluorine substituents in the same positions as the individual fluorine atoms in **S2** and **S3**. This change has extinguished the nematic phase and a direct N_F–I transition is observed, corresponding to a reduction in T_{NI} of at least 40 K compared to **S1**. In contrast, the stability of the N_F has increased again and T_{NFI} for **S4** is 23 K higher than T_{NFNX} observed for **S1**. It is also noteworthy that T_{NFI} for **S4** is higher than T_{NFN} of **S2** by 7 K and of **S3** by 3 K. The dipole moment of **S4** is 12.4 D and higher than that of either **S2** or **S3**. It is clear that the effects of the two fluorine atoms on the stability of the N_F phase are not simply additive and such a relationship would predict a T_{NFI} for **S4** of around 142 °C. The rather modest increases in the stability of the N_F phase between **S4**, and **S2** and **S3** is not immediately apparent from Madhusudana's model. If the F-substituent in **S2** acts to reduce the amplitude of the charge density on the terminal ring, and that in **S3** increases the amplitude of the charge density on the middle ring, then the combined effect in **S4** should be to increase the difference between these two amplitudes, further increasing the stability of the N_F phase. Presumably the change in molecular shape must also be considered and this will not be simply additive, nor is it straightforward to assess.

S5 also contains two fluorine substituents but both are attached to the middle aromatic ring, and these have reduced T_{NI} by 42 K compared to **S1**. The single fluorine substituent on the middle ring in **S3** reduced T_{NI} by 17 K compared to **S1**, and so the second fluorine substituent has had a more pronounced effect on T_{NI} than the first, reducing T_{NI} by 25 K. The stability of the N_F phase shown by **S5** is higher than that of **S1**, but T_{NFN} is lower than that of **S3** by 5 K even though its dipole moment of 11.8 D is higher than that of **S3** of 11.2 D. These effects may be attributed to the change in molecular shape on the addition of

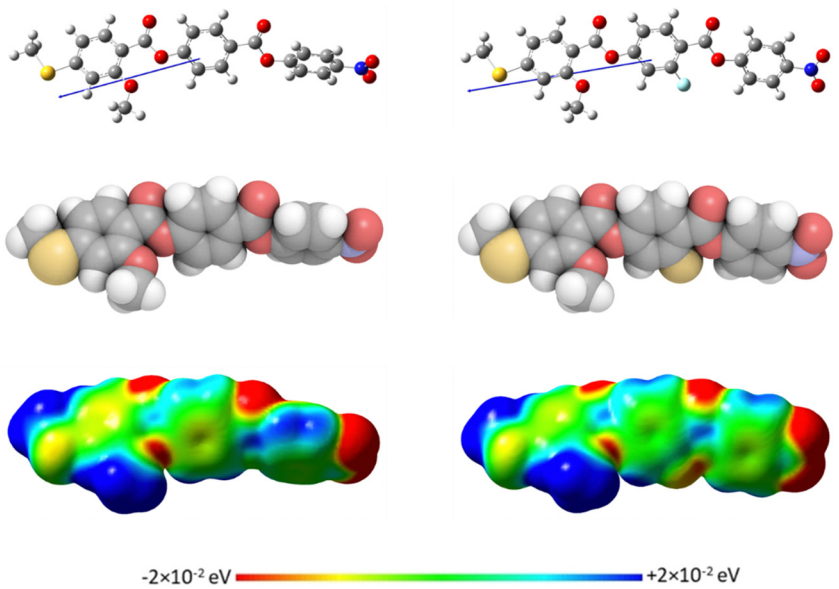

Fig. 8 Molecular modelling of: **S1** (left) and **S3** (right) calculated at the B3LYP/6-31(d) level of theory. The molecules are visualized using: (top) ball and stick models, (middle) space-filling models and (bottom) electrostatic potential surfaces. The arrow indicates the direction of the calculated dipole moment, with the head representing positive charge moving to the base which is negative.

the second fluorine substituent, and presumably this also spreads the electron distribution on the middle phenyl ring reducing the amplitude of the charge density wave relative to that of the terminal ring.

All three fluorine substituents are included in **S6**, and this has extinguished nematic behaviour in comparison to **S1** indicating a reduction in T_{NI} of at least 47 K. The value of T_{NFI} for **S6** is essentially the same as T_{NFN} shown by **S2** and **S5** although its dipole moment of 13.0 D is the highest in this collection of molecules. It is becoming increasingly apparent that the magnitude of the dipole moment alone is not a good indicator of the stability of the N_F phase. **S6** shows the largest reduction in T_{NI} compared to **S1** suggesting that the three fluorine substituents have a significant effect on molecular shape, and this presumably offsets a larger increase in the stability of the N_F phase based on the predicted increment in stability associated with the addition of the fluorine substituent on the terminal phenyl ring.

For comparative purposes, the transitional properties of the corresponding methoxy-substituted materials to **S1–6**, the **O1–6** compounds are listed in Table 2 and their structures shown in Fig. 1. **O5** and **O6** were prepared as part of this study and their phase assignments based on the observation of a characteristic schlieren texture for the nematic phase, Fig. 9(a) and a banded texture for the N_F phase similar to that which we have reported previously, Fig. 9(b).[18,20,25] For **O5** our studies have revealed a previously overlooked N phase and the characterisation data for this are provided in the ESI.† The remaining data have been extracted from the literature.[3,8,18,20] The trends in phase behaviour within these two sets of compounds, **S1–6** and **O1–6**, are similar and tend to only differ in the magnitude of the temperature differences between compounds, Fig. 10. These

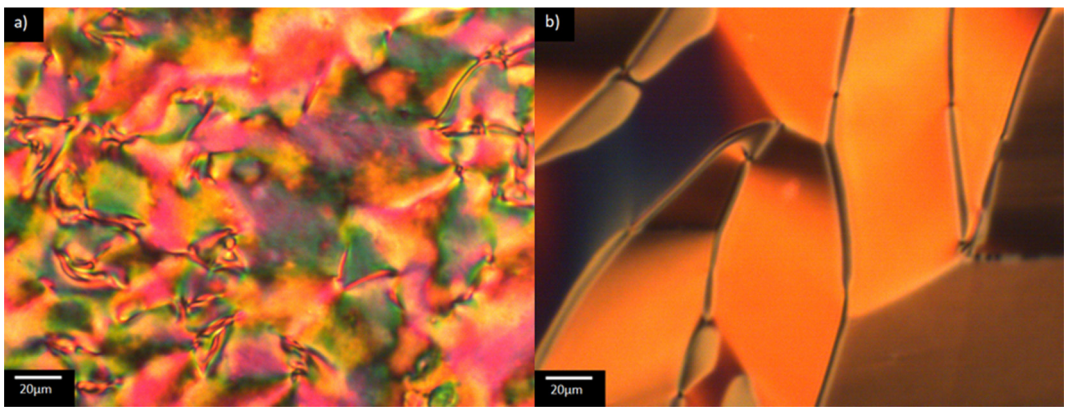

Fig. 9 Polarised optical microscope textures observed for **O6**: (a) highly birefringent texture of the N_F phase viewed between untreated glass slides at 125 °C; (b) banded texture of the N_F phase in a cell treated for planar alignment at 125 °C.

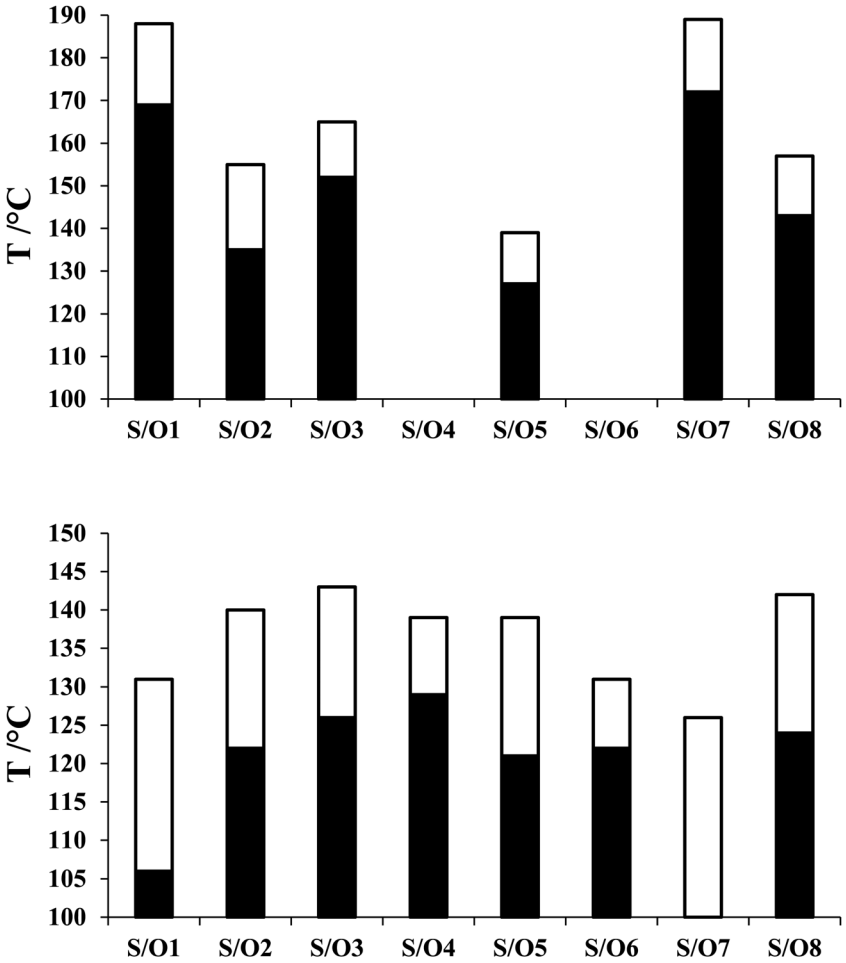

Fig. 10 Comparison of the N–I (top) and N_F–N/N_X/I (bottom) transition temperatures of the S*n* series (filled bar) and O*n* series (open bar).

temperature differences are most striking in the compounds containing more than one fluorine substituent for which the increase in the stability of the N_F phase is significantly larger in the S*n* compounds. For example, the stability of the N_F phase shown by **S6** is 16 K higher than that of **S1**, whereas the value of T_{NFI} shown by **O6** is the same as that of T_{NFN} is for **O1**. This may reflect the weaker relative effect multiple fluorine substituents have on the shape of the S*n* compounds given the larger methylthio group and we return to this issue later.

In **S7** the methoxy substituent on the terminal ring has been moved to the middle ring and this increases T_{NI} by just 3 K compared to **S1**. This small change reflects the small change in the shape anisotropy of the molecule. By contrast, T_{NXN} has fallen by 14 K and the N_F phase is no longer observed for **S7**. This suggests that the addition of the methoxy unit to the middle ring has reduced the amplitude of the charge density wave given its electron donating character. As would be expected the addition of a fluorine substituent *ortho* to the nitro group giving **S8** promotes N_F behaviour and reduces T_{NI} compared to **S7**, Fig. 10. Again, similar trends in behaviour are observed for the corresponding methoxy substituted materials **O7** and **O8**, see Table 2. The N_X phase is again not observed in the O*n* compounds.

The transitional behaviour of the corresponding S*n* and O*n* materials, Table 2, is identical except for the pairs **S1** and **O1** (RM734), and **S7** and **O7**. In both **S1** and **S7** the N_X phase is observed but not seen in the corresponding O compounds. In addition, the N_F phase is not observed for **S7** but is for **O7**. Indeed, isolated droplets of **S7** can be cooled to 60 °C with no sign of a phase change within the N_X phase, implying a reduction in T_{NFN} of at least 66 K compared to **O7**. Comparing the transition temperatures of each pair of compounds, Fig. 10, the methoxy-substituted compound consistently shows the higher values of T_{NFN}, T_{NFI} and T_{NI}. For each of the transitions, the larger methylthio group contributes to a larger reduction in shape anisotropy and accounts in part for the lower transition temperatures, Fig. 11. In addition, the calculated dipole moment of each O*n* compound is higher than that of the corresponding S*n* material. The sterically bulkier methylthio group presumably inhibits the ability of the compounds to pack together in the parallel manner found in the N_F phase.[63] The observation of the N_X phase for **S1** and **S7** may simply reflect the greater suppression of the N_F phase by the methylthio group revealing the underlying N_X phase rather than from any specific stabilising effect. The generality of these observations now requires further investigation.

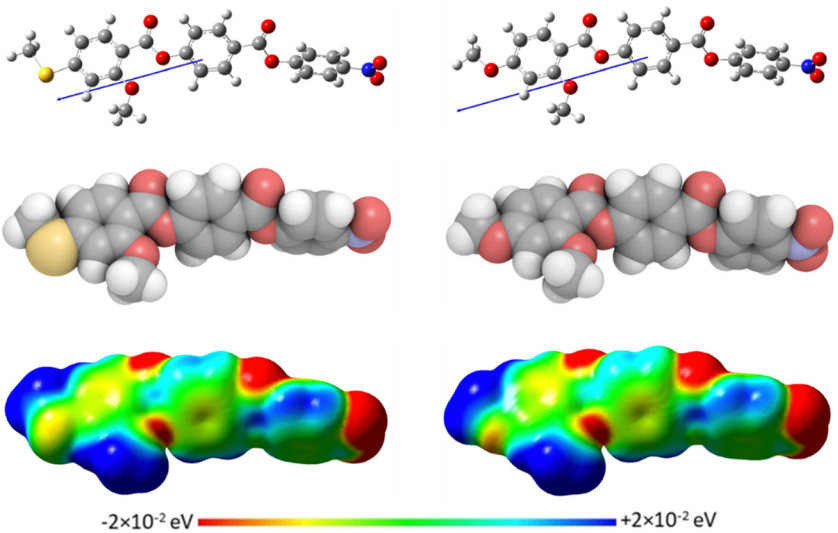

Fig. 11 Molecular modelling of: **S1** (left) and **O1** (right) calculated at the B3LYP/6-31(d) level of theory. The molecules are visualized using: (top) ball and stick models, (middle) space-filling models and (bottom) electrostatic potential surfaces. The arrow indicates the direction of the calculated dipole moment, with the head representing positive charge moving to the base which is negative.

We recently reported the properties of the ethyl substituted compound, 2EC6F (Fig. 12), corresponding to **S8** and **O8**. 2EC6F exhibits a N_F–I transition at 132 °C.[9] This implies that the decrease in T_{NI} on replacing the methoxy group by an ethyl group is at least 25 K and for the methylthio group at least 11 K. By contrast, the value of T_{NFI} is just 10 K lower than T_{NFN} of **O8** and 8 K higher than that of **S8**. At first sight the reduction in T_{NI} between **S8** and 2EC6F is surprising given that the ethyl group is more compact than the methylthio unit. We have shown, however, for other low molar mass systems that the values of T_{NI} for systems containing methylthio and ethylthio terminal groups are higher than expected based on the behaviour of longer chain homologues, and attributed this to a specific interaction between the molecules, possibly a chalcogen bond.[28] This would also account for the surprisingly high T_{NI} seen for **S8** but this interaction appears not to stabilise the N_F phase. Instead, the ethyl group is a better electron donating group than methylthio, and this decreases the amplitude of the charge density at the end of the molecule stabilising the N_F phase. This also accounts for the more stable N_F phase shown by **O8** given that the methoxy group is also a stronger electron donating group. In addition, in terms of molecule shape, the methoxy unit lies in the plane of the phenyl ring to which it is attached, whereas the ethyl group protrudes at an angle disrupting the formation of the N_F phase.

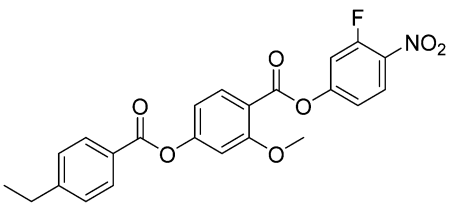

Fig. 12 Molecular structure of 2EC6F.

Conclusions

We have reported the first set of ferroelectric nematogens containing a sulfur atom, **S1–8**, specifically in the form of a methylthio group, and compared their properties to those of the corresponding materials containing a methoxy group, **O1–8**. The difference in the transition temperatures within the S*n* and O*n* series may be accounted for in terms of the change in shape and electronic properties, based on the extent of fluorination along the molecular backbone. The behaviour of these materials can be accounted for within the framework of a molecular model developed by Madhusudana.[63]

The molecular dipole moment alone, however, is not necessarily a good indicator of the stability of the N_F phase, with compounds possessing higher dipole moments exhibiting transitions to the N_F phase at lower temperatures. On comparing the properties of corresponding members of the two sets of materials, the methoxy-substituted compound consistently shows the higher values of T_{NFN}, T_{NFI} and T_{NI}. This is attributed to the larger reduction in molecular shape anisotropy associated with the methylthio group and its greater steric bulk. Evidently, the replacement of the terminal methoxy group by the methylthio group did not see a stabilisation of the N_F phase, however, the N_X phase was only observed for two compounds and both of which contained a terminal methylthio group. This may simply reflect the greater suppression of the N_F phase by the methylthio group revealing the underlying N_X phase rather than from any specific stabilising effect. A comparison using the reported behaviour of the ethyl substituted compound corresponding to **S8** and **O8** suggested that the interactions we have reported on previously,[28] in terms of methylthio terminated low molar mass mesogens, do not appear to stabilise the N_F phase, as they do for the conventional nematic phase, and this reinforces the view that molecular shape is an important factor in promoting the N_F phase.

Conflicts of interest

There are no conflicts of interest to declare.

Acknowledgements

C.T.I. and J.M.D.S. acknowledge the financial support of the Engineering and Physical Sciences Research Council [EP/V048775/1]. The research was supported by the National Science Centre (Poland) under the grant no. 2021/43/B/ST5/00240.

References

1 R. J. Mandle, S. J. Cowling and J. W. Goodby, A nematic to nematic transformation exhibited by a rod-like liquid crystal, *Phys. Chem. Chem. Phys.*, 2017, **19**, 11429–11435.
2 H. Nishikawa, K. Shiroshita, H. Higuchi, Y. Okumura, Y. Haseba, S. I. Yamamoto, K. Sago and H. Kikuchi, A Fluid Liquid-Crystal Material with Highly Polar Order, *Adv. Mater.*, 2017, **29**, 1702354.
3 R. J. Mandle, S. J. Cowling and J. W. Goodby, Rational Design of Rod-Like Liquid Crystals Exhibiting Two Nematic Phases, *Chem. – A Eur. J.*, 2017, **23**, 14554–14562.
4 X. Chen, E. Korblova, D. Dong, X. Wei, R. Shao, L. Radzihovsky, M. A. Glaser, J. E. Maclennan, D. Bedrov, D. M. Walba and N. A. Clark, First-principles experimental demonstration of ferroelectricity in a thermotropic nematic liquid crystal: Polar domains and striking electro-optics, *Proc. Natl. Acad. Sci. U. S. A.*, 2020, **117**, 14021–14031.
5 X. Chen, V. Martinez, E. Korblova, G. Freychet, M. Zhernenkov, M. A. Glaser, C. Wang, C. Zhu, L. Radzihovsky, J. E. Maclennan, D. M. Walba and N. A. Clark, The smectic ZA phase: Antiferroelectric smectic order as a prelude to the ferroelectric nematic, *Proc. Natl. Acad. Sci. U. S. A.*, 2022, **120**, e2217150120.
6 Y. Song, M. Deng, Z. Wang, J. Li, H. Lei, Z. Wan, R. Xia, S. Aya and M. Huang, Emerging Ferroelectric Uniaxial Lamellar (Smectic AF) Fluids for Bistable In-Plane Polarization Memory, *J. Phys. Chem. Lett.*, 2022, **13**, 9983–9990.
7 X. Chen, V. Martinez, P. Nacke, E. Korblova, A. Manabe, M. Klasen-Memmer, G. Freychet, M. Zhernenkov, M. A. Glaser, L. Radzihovsky, J. E. Maclennan, D. M. Walba, M. Bremer, F. Giesselmann, N. A. Clark, N. Abbott and P. Palffy-Muhoray, Observation of a uniaxial ferroelectric smectic A phase, *Proc. Natl. Acad. Sci. U. S. A.*, 2022, **119**, e2210062119.
8 S. Brown, E. Cruickshank, J. M. D. Storey, C. T. Imrie, D. Pociecha, M. Majewska, A. Makal and E. Gorecka, Multiple Polar and Non-polar Nematic Phases, *Chem. Phys. Chem.*, 2021, **22**, 2506–2510.
9 E. Cruickshank, P. Rybak, M. M. Majewska, S. Ramsay, C. Wang, C. Zhu, R. Walker, J. M. D. Storey, C. T. Imrie, E. Gorecka and D. Pociecha, To be or not to be polar: the ferroelectric and antiferroelectric nematic phases, *ACS Omega*, 2023, **8**, 36562–36568.
10 J. Li, R. Xia, H. Xu, J. Yang, X. Zhang, J. Kougo, H. Lei, S. Dai, H. Huang, G. Zhang, F. Cen, Y. Jiang, S. Aya and M. Huang, How Far Can We Push the Rigid Oligomers/Polymers toward Ferroelectric Nematic Liquid Crystals?, *J. Am. Chem. Soc.*, 2021, **143**, 46.
11 S. Dai, J. Li, J. Kougo, H. Lei, S. Aya and M. Huang, Polar Liquid Crystalline Polymers Bearing Mesogenic Side Chains with Large Dipole Moment, *Macromolecules*, 2021, **54**, 6045–6051.
12 D. Pociecha, R. Walker, E. Cruickshank, J. Szydlowska, P. Rybak, A. Makal, J. Matraszek, J. M. Wolska, J. M. D. Storey, C. T. Imrie and E. Gorecka, Intrinsically chiral ferronematic liquid crystals: an inversion of the helical twist sense at the chiral nematic – chiral ferronematic phase transition, *J. Mol. Liq.*, 2021, **361**, 119532.
13 J. Li, H. Nishikawa, J. Kougo, J. Zhou, S. Dai, W. Tang, X. Zhao, Y. Hisai, M. Huang and S. Aya, Development of ferroelectric nematic fluids with giant-dielectricity and nonlinear optical properties, *Sci. Adv.*, 2021, **7**, eabf5047.
14 J. Li, Z. Wang, M. Deng, Y. Zhu, X. Zhang, R. Xia, Y. Song, Y. Hisai, S. Aya and M. Huang, General Phase-structure Relationship in Polar Rod-shaped Liquid Crystals: Importance of Shape Anisotropy and Dipolar Strength, *Giant*, 2022, **11**, 100109.
15 R. Saha, P. Nepal, C. Feng, M. S. Hossain, M. Fukuto, R. Li, J. T. Gleeson, S. Sprunt, R. J. Twieg and A. Jákli, Multiple ferroelectric nematic phases of a highly polar liquid crystal compound, *Liq. Cryst.*, 2022, **49**, 1784–1796.
16 A. Manabe, M. Bremer and M. Kraska, Ferroelectric nematic phase at and below room temperature, *Liq. Cryst.*, 2021, **48**, 1079–1086.
17 N. Sebastián, R. J. Mandle, A. Petelin, A. Eremin and A. Mertelj, Electrooptics of mm-scale polar domains in the ferroelectric nematic phase, *Liq. Cryst.*, 2021, **48**, 2055–2071.
18 N. Tufaha, E. Cruickshank, D. Pociecha, E. Gorecka, J. M. D. Storey and C. T. Imrie, Molecular Shape, Electronic Factors and the Ferroelectric Nematic Phase, *Chem. – A Eur. J.*, 2023, **29**, e202300073.
19 J. Zhou, R. Xia, M. Huang and S. Aya, Stereoisomer effect on ferroelectric nematics: stabilization and phase behavior diversification, *J. Mater. Chem. C*, 2022, **10**, 8762–8766.
20 E. Cruickshank, R. Walker, J. M. D. Storey and C. T. Imrie, The effect of a lateral alkyloxy chain on the ferroelectric nematic phase, *RSC Adv.*, 2022, **12**, 29482–29490.
21 H. Kikuchi, H. Matsukizono, K. Iwamatsu, S. Endo, S. Anan and Y. Okumura, Fluid Layered Ferroelectrics with Global C∞v Symmetry, *Adv. Sci.*, 2022, **9**, 2202048.
22 R. J. Mandle, A new order of liquids: polar order in nematic liquid crystals, *Soft Matter*, 2022, **18**, 5014–5020.
23 N. Sebastián, M. Čopič and A. Mertelj, Ferroelectric nematic liquid-crystalline phases, *Phys. Rev. E*, 2022, **106**, 021001.
24 Y. Song, J. Li, R. Xia, H. Xu, X. Zhang, H. Lei, W. Peng, S. Dai, S. Aya and M. Huang, Development of emergent ferroelectric nematic liquid crystals with highly fluorinated and rigid mesogens, *Phys. Chem. Chem. Phys.*, 2022, **24**, 11536–11543.
25 E. Cruickshank, A. Pearson, S. Brown, J. M. D. Storey, C. T. Imrie and R. Walker, The ferroelectric nematic phase:

on the role of lateral alkyloxy chains, *Liq. Cryst.*, 2023, DOI: 10.1080/02678292.2023.2221651.
26 R. Berardi, M. Ricci and C. Zannoni, Ferroelectric nematic and smectic liquid crystals from tapered molecules, *ChemPhysChem*, 2001, **2**, 443–447.
27 R. J. Mandle, Supramolecular ferroelectric nematic materials, *Liq. Cryst.*, 2022, **49**, 2019–2026.
28 E. Cruickshank, G. J. Strachan, J. M. D. Storey and C. T. Imrie, Chalcogen bonding and liquid crystallinity: Understanding the anomalous behaviour of the 4′-(alkylthio)[1,1′-biphenyl]-4-carbonitriles (nSCB), *J. Mol. Liq.*, 2021, **346**, 117094.
29 Y. Arakawa, S. Inui and H. Tsuji, Synthesis, phase transitions, and liquid crystal behavior of alkylthio azobenzenes, *Tetrahedron*, 2022, **122**, 132958.
30 Y. Arakawa, S. Inui, K. Igawa and H. Tsuji, Alkylthio- and alkyl-substituted asymmetric diphenyldiacetylene-based liquid crystals: phase transitions, mesophase and single-crystal structures, and birefringence, *Liq. Cryst.*, 2019, **46**, 1621–1630.
31 Y. Arakawa, Y. Ishida, Y. Sasaki, S. Sasaki, M. Tokita and H. Tsuji, Alkylthio-based asymmetric liquid crystals: unravelling the substituent effects and intercalated cybotactic nematic and smectic phases, *Mater. Adv.*, 2022, **3**, 3218–3228.
32 M. Alaasar, A. F. Darweesh, X. Cai, F. Liu and C. Tschierske, Mirror Symmetry Breaking and Network Formation in Achiral Polycatenars with Thioether Tail, *Chem. – A Eur. J.*, 2021, **27**, 14921–14930.
33 Y. Arakawa, S. Kang, J. Watanabe and G. I. Konishi, Assembly of thioether-containing rod-like liquid crystalline materials assisted by hydrogen-bonding terminal carboxyl groups, *RSC Adv.*, 2015, **5**, 8056–8062.
34 E. Cruickshank, G. J. Strachan, M. M. Majewska, D. Pociecha, E. Górecka, J. M. D. Storey and C. T. Imrie, The effects of alkylthio chains on the properties of symmetric liquid crystal dimers, *New J. Chem.*, 2023, **47**, 7356–7368.
35 E. Cruickshank, M. Salamończyk, D. Pociecha, G. J. Strachan, J. M. D. Storey, C. Wang, J. Feng, C. Zhu, E. Gorecka and C. T. Imrie, Sulfur-linked cyanobiphenyl-based liquid crystal dimers and the twist-bend nematic phase, *Liq. Cryst.*, 2019, **46**, 1595–1609.
36 Y. Arakawa, K. Komatsu and H. Tsuji, Twist-bend nematic liquid crystals based on thioether linkage, *New J. Chem.*, 2019, **43**, 6786–6793.
37 K. Isoda, T. Ichikawa, K. Kaneko, M. Kondo, T. Sakurai, A. Seki, M. Hara, G. Watanabe, Y. Arakawa, Y. Arai, K. Horita, K. Komatsu and H. Tsuji, Twist-Bend Nematic Phase Behavior of Cyanobiphenyl-Based Dimers with Propane, Ethoxy, and Ethylthio Spacers, *Crystals*, 2022, **12**, 1734.
38 Y. Arakawa, K. Komatsu, Y. Ishida, T. Shiba and H. Tsuji, Thioether-Linked Liquid Crystal Trimers: Odd–Even Effects of Spacers and the Influence of Thioether Bonds on Phase Behavior, *Materials*, 2022, **15**, 1709.
39 Y. Arakawa, K. Komatsu, S. Inui and H. Tsuji, Thioether-linked liquid crystal dimers and trimers: The twist-bend nematic phase, *J. Mol. Struct.*, 2020, **1199**, 126913.
40 Y. Arakawa, K. Komatsu, T. Shiba and H. Tsuji, Methylene- and thioether-linked cyanobiphenyl liquid crystal dimers CB*n* SCB exhibiting room temperature twist-bend nematic phases and glasses, *Mater. Adv.*, 2021, **2**, 1760–1773.
41 A. J. Seed, K. J. Toyne and J. W. Goodby, Synthesis of some 2,4- and 2,5-disubstituted thiophene systems and the effect of the pattern of substitution on the refractive indices, optical anisotropies, polarisabilities and order parameters in comparison with those of the parent biphenyl and dithien, *J. Mater. Chem.*, 1995, **5**, 653–661.
42 A. Seed, Synthesis of self-organizing mesogenic materials containing a sulfur-based five-membered heterocyclic core, *Chem. Soc. Rev.*, 2007, **36**, 2046–2069.
43 M. K. Reddy, K. S. Reddy, M. Prakash and T. Narasimhaswamy, Synthesis and Characterization of Two Phenyl Ring Core-Based Thiophene Mesogens, *Mol. Cryst. Liq. Cryst.*, 2013, **582**, 1–14.
44 Y. Arakawa, S. Kang, S. Nakajima, K. Sakajiri, S. Kawauchi, J. Watanabe and G. Konishi, Synthesis of new wide nematic diaryl-diacetylenes containing thiophene-based heteromonocyclic and heterobicyclic structures, and their birefringence properties, *Liq. Cryst.*, 2014, **41**, 642–651.
45 M. Hird, A. J. Seed, K. J. Toyne, J. W. Goodby, G. W. Gray and D. G. McDonnell, Synthesis, transition temperatures and optical anisotropy of some isothiocyanato-substituted biphenyls, *J. Mater. Chem.*, 1993, **3**, 851–859.
46 G. J. Cross, A. J. Seed, K. J. Toyne, J. W. Goodby, M. Hird and M. C. Artal, Synthesis, transition temperatures, and optical properties of compounds with simple phenyl units linked by double bond, triple bond, ester or propiolate linkages, *J. Mater. Chem.*, 2000, **10**, 1555–1563.
47 A. J. Seed, K. J. Toyne, J. W. Goodby and D. G. McDonnell, Synthesis, optical anisotropies, polarisabilities and order parameters of 4-cyanophenyl and 4-isothiocyanatophenyl 4′-butylsulfanylbenzoates with oxygen and sulfur substitution in the ester linkage, *J. Mater. Chem.*, 1995, **5**, 1–11.
48 Z. Fang and C. Wu, Investigation on thermal behaviour and optical properties of non-symmetric cholesterol-based twin liquid crystals with thioester linkages, *Liq. Cryst.*, 2020, **47**, 1086–1099.
49 Y. Arakawa, Y. Sasaki, N. Haraguchi, S. Itsuno and H. Tsuji, Synthesis, phase transitions and birefringence of novel liquid crystalline 1,4-phenylene bis(4-alkylthio benzoates) and insights into the cybotactic nematic behaviour, *Liq. Cryst.*, 2018, **45**, 821–830.
50 Y. Arakawa and H. Tsuji, Phase transitions and birefringence of bistolane-based nematic molecules with an alkyl, alkoxy and alkylthio group, *Mol. Cryst. Liq. Cryst.*, 2017, **647**, 422–429.
51 Y. Arakawa and H. Tsuji, Selenium-linked liquid crystal dimers for twist-bend nematogens, *J. Mol. Liq.*, 2019, **289**, 111097.
52 Y. Arakawa, H. Kuwahara, M. Tokita and G. Konishi, ichi & Tsuji, H. New fabrication approach to develop a high birefringence photo-crosslinked film based on a sulfur-containing liquid crystalline molecule with large temperature dependence of birefringence, *Mol. Cryst. Liq. Cryst.*, 2018, **662**, 197–207.
53 H. R. H. R. Stapert, S. Del Valle, E. J. K. Verstegen, B. M. I. Van der Zande, J. Lub and S. Stallinga, Photoreplicated

Anisotropic Liquid-Crystalline Lenses for Aberration Control and Dual-Layer Readout of Optical Discs, *Adv. Funct. Mater.*, 2003, **13**, 732–738.

54 I. M. Syed, S. Kaur, H. E. Milton, D. Mistry, J. Bailey, P. B. Morgan, J. Cliff Jones, H. F. Gleeson, H. E. Milton, P. B. Morgan, J. H. Clamp, H. F. Gleeson, J. C. Jones and H. F. Gleeson, Novel switching mode in a vertically aligned liquid crystal contact lens, *Opt. Express*, 2015, **23**, 9911–9916.

55 N. Kawatsuki, A. Yamashita, M. Kondo, T. Matsumoto, T. Shioda, A. Emoto and H. Ono, Photoinduced reorientation and polarization holography in photo-cross-linkable liquid crystalline polymer films with large birefringence, *Polymer*, 2010, **51**, 2849–2856.

56 M. J. Frisch, G. W. Trucks, H. B. Schlegel, G. E. Scuseria, M. A. Robb, J. R. Cheeseman, G. Scalmani, V. Barone, B. Mennucci, G. A. Petersson, H. Nakatsuji, M. Caricato, X. Li, H. P. Hratchian, A. F. Izmaylov, J. Bloino, G. Zheng, J. L. Sonnenberg, M. Hada, M. Ehara, K. Toyota, R. Fukuda, J. Hasegawa, M. Ishida, T. Nakajima, Y. Honda, O. Kitao, H. Nakai, T. Vreven, J. A. Montgomery, J. E. Peralta, F. Ogliaro, M. Bearpark, J. J. Heyd, E. Brothers, K. N. Kudin, V. N. Staroverov, R. Kobayashi, J. Normand, K. Raghavachari, A. Rendell, J. C. Burant, S. S. Iyengar, J. Tomasi, M. Cossi, N. Rega, J. M. Millam, M. Klene, J. E. Knox, J. B. Cross, V. Bakken, C. Adamo, J. Jaramillo, R. Gomperts, R. E. Stratmann, O. Yazyev, A. J. Austin, R. Cammi, C. Pomelli, J. W. Ochterski, R. L. Martin, K. Morokuma, V. G. Zakrzewski, G. A. Voth, P. Salvador, J. J. Dannenberg, S. Dapprich, A. D. Daniels, J. B. Farkas Foresman, J. V. Ortiz, J. Cioslowski and D. J. Fox, *Gaussian 09, Revision B.01*, Gaussian, Inc., Wallingford CT. (2010).

57 M. Tarini, P. Cignoni and C. Montani, Ambient occlusion and edge cueing to enhance real time molecular visualization, *IEEE Trans. Vis. Comput. Graph.*, 2006, **12**, 1237–1244.

58 H. Nishikawa, K. Sano, S. Kurihara, G. Watanabe, A. Nihonyanagi, B. Dhara and F. Araoka, Nano-clustering mediates phase transitions in a diastereomerically-stabilized ferroelectric nematic system, *Commun. Mater.*, 2022, **3**, 89.

59 H. Nishikawa, K. Sano and F. Araoka, Anisotropic fluid with phototunable dielectric permittivity, *Nat. Commun.*, 2022, **13**, 1142.

60 X. Zhao, J. Zhou, J. Li, J. Kougo, Z. Wan, M. Huang and S. Aya, Spontaneous helielectric nematic liquid crystals: Electric analog to helimagnets, *Proc. Natl. Acad. Sci. U. S. A.*, 2021, **118**, e2111101118.

61 A. Erkoreka, J. Martinez-Perdiguero, R. J. Mandle, A. Mertelj and N. Sebastián, Dielectric spectroscopy of a ferroelectric nematic liquid crystal and the effect of the sample thickness, *J. Mol. Liq.*, 2023, **387**, 122566.

62 X. Chen, Z. Zhu, M. J. Magrini, E. Korblova, C. S. Park, M. A. Glaser, J. E. Maclennan, D. M. Walba and N. A. Clark, Ideal mixing of paraelectric and ferroelectric nematic phases in liquid crystals of distinct molecular species, *Liq. Cryst.*, 2022, **49**, 1531–1544.

63 N. V. Madhusudana, Simple molecular model for ferroelectric nematic liquid crystals exhibited by small rodlike mesogens, *Phys. Rev. E*, 2021, **104**, 014704.